

SHORT REPORTS

Active mode of excretion across digestive tissues predates the origin of excretory organs

Carmen Andrikou¹*, Daniel Thiel¹, Juan A. Ruiz-Santesteban¹, Andreas Hejnol¹*

Sars International Centre for Marine Molecular Biology, University of Bergen, Bergen, Norway

* carmen.andrikou@uib.no (CA); andreas.hejnol@uib.no (AH)



OPEN ACCESS

Citation: Andrikou C, Thiel D, Ruiz-Santesteban JA, Hejnol A (2019) Active mode of excretion across digestive tissues predates the origin of excretory organs. PLoS Biol 17(7): e3000408. <https://doi.org/10.1371/journal.pbio.3000408>

Academic Editor: Claude Desplan, New York University, UNITED STATES

Received: April 15, 2019

Accepted: July 12, 2019

Published: July 29, 2019

Copyright: © 2019 Andrikou et al. This is an open access article distributed under the terms of the [Creative Commons Attribution License](https://creativecommons.org/licenses/by/4.0/), which permits unrestricted use, distribution, and reproduction in any medium, provided the original author and source are credited.

Data Availability Statement: All newly determined sequences have been deposited in GenBank under accession numbers MN101600—MN101702. The assembled xenacoelomorph transcriptomes used for the gene orthology assessment are deposited on Dryad Digital Depository: <https://doi.org/10.5061/dryad.bq068jr> [72].

Funding: The study was supported by the European Research Council Community's Framework Program Horizon 2020 (2014–2020) ERC grant agreement 648861 (EVOMESODERM)

Abstract

Most bilaterian animals excrete toxic metabolites through specialized organs, such as nephridia and kidneys, which share morphological and functional correspondences. In contrast, excretion in non-nephrozoans is largely unknown, and therefore the reconstruction of ancestral excretory mechanisms is problematic. Here, we investigated the excretory mode of members of the Xenacoelomorpha, the sister group to Nephrozoa, and Cnidaria, the sister group to Bilateria. By combining gene expression, inhibitor experiments, and exposure to varying environmental ammonia conditions, we show that both Xenacoelomorpha and Cnidaria are able to excrete across digestive-associated tissues. However, although the cnidarian *Nematostella vectensis* seems to use diffusion as its main excretory mode, the two xenacoelomorphs use both active transport and diffusion mechanisms. Based on these results, we propose that digestive-associated tissues functioned as excretory sites before the evolution of specialized organs in nephrozoans. We conclude that the emergence of a compact, multiple-layered bilaterian body plan necessitated the evolution of active transport mechanisms, which were later recruited into the specialized excretory organs.

Introduction

Excretory organs are specialized organs that remove toxic metabolic waste products and control water and ion balance in animals based on the principles of ultrafiltration, active transport, and passive transport/diffusion [1]. They are only present in Nephrozoa (Deuterostomia + Protostomia) [2] (Fig 1a) and, based on morphological correspondences, can be grouped into two major architectural units: the protonephridia, only found in Protostomia, and the metanephridia, present in both Deuterostomia and Protostomia [3,4]. Both organs are organized into functionally similar compartments: the terminal cells of protonephridia and the podocytes associated to metanephridial systems conduct ultrafiltration, and the tubule and duct cells modify the filtrate through a series of selective reabsorption and secretion, via passive and active transport mechanisms [5] (Fig 1b). There exist also other, taxon-specific excretory organs and excretory sites, which perform either ultrafiltration (such as the nephrocytes of

(<https://cordis.europa.eu/project/rcn/197107/factsheet/en>) and FP7-PEOPLE-2012-ITN grant no. 317172 (NEPTUNE) (<https://cordis.europa.eu/project/rcn/104658/factsheet/en>) to AH and Coca-Cola Foundation (<https://www.coca-colacompany.com/our-company/the-coca-cola-foundation>) to JAR-S. The funders had no role in study design, data collection and analysis, decision to publish, or preparation of the manuscript.

Competing interests: The authors have declared that no competing interests exist.

Abbreviations: AMT, ammonia transporter; CA, carbonic anhydrase; cd2ap, CD2-associated protein; cu, cuticle; HCN, $K^+[NH_4^+]$ channel; HEA, high environmental ammonia; NKA, $Na^+/K^+[NH_4^+]$ ATPase; qPCR, quantitative PCR; Rh, Rhesus glycoprotein; SLC, solute carrier transporter; v-ATPase, vacuolar H^+ -ATPase proton pump; WMISH, whole-mount in situ hybridization; zo1, zonula occludens 1.

insects [6] and the rhogocytes of gastropods [7] or absorption and secretion (such as the malpighian tubules of various tardigrades, arachnids, and insects [8]; the excretory cells of nematodes [9]; the gills of fish, shore crabs, and annelids [10,11]; and the epidermis of planarians [12]).

Molecular studies have shown that a suite of orthologous genes is involved in the excretory mechanisms of different nephrozoan species, regardless of whether they possess specialized excretory organs [9–12,14–31] (see also [S1 Table](#)). The passive ammonia transporters Rhesus/AMTs, the active transporter $Na^+/K^+[NH_4^+]$ ATPase (NKA), the hyperpolarization-activated cyclic nucleotide-gated $K^+[NH_4^+]$ channels (HCN), the vacuolar H^+ -ATPase (v-ATPase subunits A and B), members of the alpha-carbonic anhydrase (CA) group, and the water/glycerol/ammonia channels (aquaporins) are commonly used for excreting ammonia, the most toxic metabolite ([Fig 1c](#)) (summarized in [5,32]). Also, a group of orthologous slit diaphragm structural components (nephrin/kirre, CD2-associated protein [cd2ap], zonula occludens 1 [zo1], stomatin/podocin), whose function is associated with the maintenance of the ultrafiltration apparatus by interacting with the actin cytoskeleton and forming tight junctions [33], is localized at the ultrafiltration site of the podocytes of the rodent kidney [34] ([Fig 1b](#)) as well as at the *Drosophila* nephrocytes [35] and the rhogocytes of gastropods [7]. Finally, a number of ion transporters (solute carrier transporters [SLCs]) are spatially expressed in the corresponding compartments of protonephridia of planarians and metanephridia (e.g., kidneys) of vertebrates [36–38] ([Fig 1b](#)).

The excretory sites and mechanisms in non-nephrozoans, however, are largely unknown. It is commonly stated that excretion is presumably occurring via diffusion across the body wall because of the loose (e.g., sponges) or single-epithelial (cnidarians and ctenophores) cellular organization of these animals [1,39,40] ([Fig 1a](#)) (herein stated as “diffusion hypothesis”). Based on this idea, it was hypothesized that the emergence of the first excretory organs coincided with the evolution of multilayered, solid parenchymes and increased body sizes because of the need of more elaborate excretory mechanisms [41,42]. However, because excretion in non-nephrozoans was never investigated in detail, the ancestral mechanisms of excretion and the evolutionary origin of excretory organs remain unresolved [1,41–46].

An important animal group for our understanding nephrozoan evolution is their bilaterian sister group [2,13,47], the Xenacoelomorpha (*Xenoturbella* + [Nemertodermatida + Acoela]). These small, worm-like animals exhibit a bilaterally symmetric, multilayered body plan, but except for a special cell type with a putative excretory function (dermonephridia) [48] that seems unique to the acoel *Paratomella*, xenacoelomorphs lack excretory organs and no defined excretory sites have yet been described. To understand the excretory mechanisms outside Nephrozoa and gain insights into ancient excretory mechanisms, we therefore investigated the excretory modes of two xenacoelomorph species and compared our findings with the non-bilaterian cnidarian *Nematostella vectensis*.

Results

Most genes involved in excretion in nephrozoa are already present in non-nephrozoan and non-bilaterian animals

To get an overview of the presence of excretion-related genes in xenacoelomorphs and non-bilaterian animals, we first searched for the orthologous sequences of 20 nephrozoan candidate genes in the available transcriptomes and draft genomes of 13 xenacoelomorph species as well as in representatives of cnidarians, placozoans, and sponges ([S1a](#) and [S2 Figs](#)). We found that most of these genes were present in almost all groups with the exceptions of *slc5* (a sodium glucose cotransporter), which was only present in Cnidaria and Bilateria, and the ultrafiltration

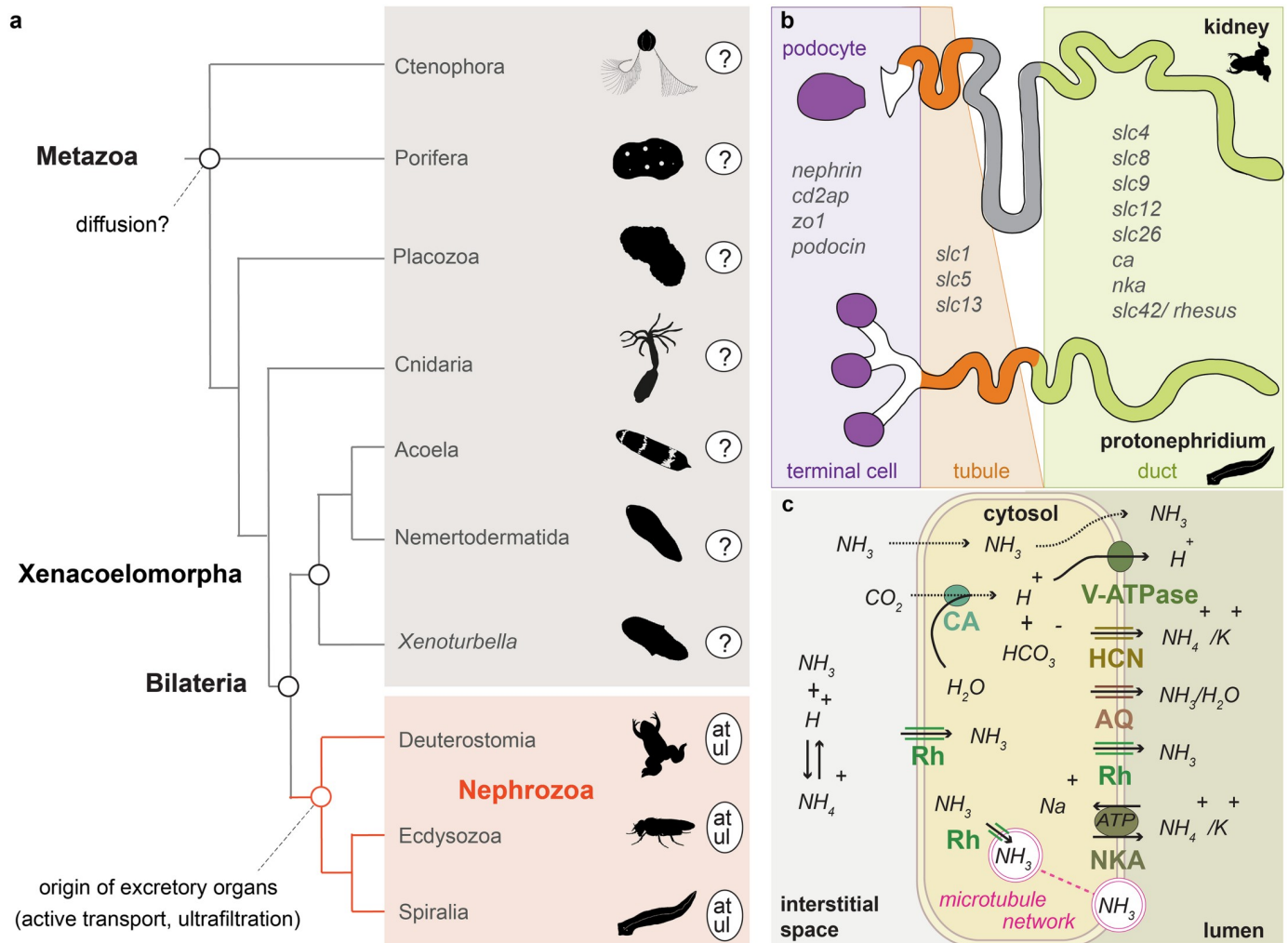


Fig 1. Traditional diffusion hypothesis, ammonia transport mechanism, and structural and functional correspondences between protonephridial and metanephridial systems. (a) Illustrated phylogenetic relationship between Nephrozoa, Xenacoelomorpha, and non-bilaterians [13]. Excretory organs or specialized excretory cells/tissues using active transport and ultrafiltration are so far only reported in the group of Nephrozoa. (b) Cartoon depiction of the structural components of metanephridia (podocyte, duct, tubule) in comparison to protonephridia (terminal cell, duct, tubule) and summary of the expression domains of orthologous selected genes in relation to their components. (c) NH_3 cellular transport. NH_3 is secreted into the lumen fluid via parallel H^+ and NH_3 transport. This involves passive diffusion through the cell membrane (dashed lines), facilitated diffusion via the Rh, active transport via the NKA, the hyperpolarization-activated cyclic nucleotide-gated HCN, and AQ as well as the generation of H^+ gradient by a v-ATPase and the CA, which transforms CO_2 into H^+ and HCO_3^- . Vesicular ammonia-trapping mechanism is also illustrated. at, active transport; AQ, aquaporin transporter; CA, carbonic anhydrase; cd2ap, CD2-associated protein; HCN, $K^+[NH_4^+]$ channel; NH_3 , ammonia; NKA, $Na^+/K^+[NH_4^+]$ ATPase; Rh, Rhesus glycoprotein; slc, solute carrier transporter; ul, ultrafiltration; v-ATPase, vacuolar H^+ -ATPase proton pump; zo1, zonula occludens 1. Animal depictions are from phylopic.org and are not copyright protected (Public Domain Mark 1.0 license).

<https://doi.org/10.1371/journal.pbio.3000408.g001>

component *nephrin/kirre*, which was only present in Bilateria (S1 Table, S1a Fig). This analysis also revealed that the last common ancestor of placozoans, cnidarians, and bilaterians already had at least two paralogs of *amts* (*amt2/3* and *am1/4*) and one *rhesus*, with independent duplications of one or both of these genes in various animal lineages (S2 Fig). To identify potential excretory sites in xenacoelomorphs, we examined the expression of the entire set of these candidate excretion-related genes in the acoel *Isodiametra pulchra* and the nemertodermatid *Meara stichopi*, which differ in their digestive system composition (*I. pulchra* has a syncytial, lumenless gut, whereas *M. stichopi* has an epithelia-lined, cellular gut [49] (S1b Fig).

Genes encoding slit diaphragm-related components and SLCs are expressed broadly in *I. pulchra* and *M. stichopi*

Genes related to ultrafiltration sites (*nephrin/kirre*, *cd2ap*, *zo1*, *stomatin/podocin*) and SLCs (*slc1*, *slc4*, *slc5*, *slc8*, *slc9*, *slc12*, *slc13*, *slc26*) were broadly expressed within neural (brain and nerve cords), parenchymal/subepidermal, digestive, and gonadal-associated cells in both animals (S3 and S4 Figs). A summary of these expression patterns is summarized in Table 1. The broad expression of ultrafiltration-related components and SLCs in acoelomorphs shows that they are not part of defined excretory domains, as in nephrozoans, thus suggesting that the spatial arrangement of these genes resulting in the formation of specialized excretory compartments (e.g., nephridial compartments) took place in the nephrozoan lineage.

The expression of a number of ammonia excretion-related genes and aquaporins suggests digestive-associated domains as putative excretion sites in *I. pulchra* and *M. stichopi*

Genes involved in ammonia excretion (*rhesus/amts*, *nka*, *v-ATPase B*, *ca*, *hcn*) and *aquaporins* were mainly demarcating neural, digestive-associated, and other parenchymal/subepidermal cells, as well as epidermal cells (Fig 2a, S4 and S5 Figs). A summary of these expression patterns is summarized in Table 1. The expression of ammonia excretion-related genes and *aquaporins* shows that these genes do not label demarcated excretory domains. However, because transcripts of the ammonium transporters *rhesus*, *nka*, and *hcn* (only in *M. stichopi*), the proton exchanger *v-ATPase*, as well as a number of *cas* and *aquaporins*, were found in association with the digestion system, the possibility that digestive-associated tissues could act as excretory sites was raised.

High environmental ammonia exposure indicates a diffusion mechanism in *I. pulchra*

To reveal the excretory mechanism in xenacoelomorphs, we conducted high environmental ammonia (HEA) incubation experiments, as previously performed in a large array of animals (summarized in [5,50]), using *I. pulchra* because of its availability in sufficient numbers. We first measured the pH of incubation mediums with different HEA concentrations (up to 1 mM) and found no difference in pH, which could otherwise have influenced any excretion rates. We then exposed animals to different HEA concentrations for a short period (2 hours) and measured the ammonia excretion during the following 2 hours, after bringing them back into normal conditions, to test excretion via diffusion. The ammonia excretion rates of exposed animals remained unchanged after exposure to 50 and 100 μM NH_4Cl , compared with the control conditions, but increased gradually after exposure to NH_4Cl concentrations of 200 and 500 μM NH_4Cl (Fig 2b). The increase in ammonia excretion rate could be explained by a concentration-dependent ammonia uptake during the HEA exposure and a subsequent release in normal conditions. These results suggest that ammonia excretion is concentration-dependent, which is indicative of a diffusion mechanism.

HEA exposure influences the expression of some excretion-related genes in *I. pulchra*

To test for a possible involvement of the excretion-related genes in the excretory mechanism of xenacoelomorphs, we tested for alteration of mRNA expression levels in chronically HEA-exposed animals by quantitative relative expression experiments (quantitative PCR [qPCR]) in *I. pulchra*. We first exposed animals to 1 mM HEA for 7 days, similar to conditions used in

Table 1. Summary of expression patterns of excretion-related genes in *I. pulchra* and *M. stichopi*.

	<i>I. pulchra</i>	<i>M. stichopi</i>
<i>nephrin/kirre</i>	<i>nephrin/kirre1</i> : brain, male gonopore	<i>nephrin/kirre1</i> : proximal lateral rows (nerve cords?)
	<i>nephrin/kirre2</i> : scattered cells (neurons?)	<i>nephrin/kirre2</i> : proximal lateral rows (nerve cords?)
	<i>nephrin/kirre3</i> : scattered cells (neurons?)	<i>nephrin/kirre3</i> : proximal lateral rows (nerve cords?)
<i>cd2ap</i>	scattered cells (neurons?)	subepidermal cells, mouth, posterior lateral rows of cells
<i>zo1</i>	scattered cells (neurons?), mouth, anterior cells (brain?)	gut-affiliated cells, mouth
<i>stom/pod</i>	<i>stom/pod a</i> : brain	<i>stom/pod a</i> : subepidermal cells, proximal lateral rows (nerve cords?)
	<i>stom/pod b</i> : digestive syncytium	<i>stom/pod b</i> : subepidermal cells, mouth
	<i>stom/pod c</i> : brain	<i>stom/pod c</i> : subepidermal cells
		<i>stom/pod d</i> : subepidermal cells
		<i>stom/pod e</i> : proximal lateral rows (nerve cords?)
<i>rhesus</i>	anterior cells, gut-affiliated cells, posterior ventral epidermis	
<i>hcn</i>	brain	gut-affiliated cells
<i>amts</i>	<i>amt-like</i> : brain	epidermis
	<i>amt1/4 a</i> : brain, mouth	
	<i>amt1/4 b</i> : parenchymal cells	
	<i>amt2/3 a</i> : scattered cells (neurons?)	
	<i>amt2/3 b</i> : brain, parenchyme	
	<i>amt2/3 c</i> : scattered cells (neurons?)	
<i>nka</i>	<i>nka a</i> : gut-wrapping cells	gut-affiliated cells
	<i>nka b</i> : gut-wrapping cells	
<i>v-ATPase B</i>	digestive syncytium	<i>v-ATPase B1</i> : gut-affiliated cells, proximal lateral rows (nerve cords?)
		<i>v-ATPase B2</i> : gut-affiliated cells, subepidermal cells
<i>alpha-ca</i>	<i>ca a</i> : anterior cells, male gonopore, mouth, parenchymal cells	<i>ca a</i> : gut-affiliated cells
	<i>ca b</i> : scattered cells (neurons?)	<i>ca b</i> : gut-wrapping cells
	<i>ca c</i> : scattered cells (neurons?)	<i>ca c</i> : gut-affiliated cells
	<i>ca d</i> : anterior cells, parenchymal cells	<i>ca d</i> : scattered cells (neurons?), posterior epidermis
	<i>ca h</i> : scattered cells (neurons?)	
	<i>ca x</i> : brain	
<i>aqs</i>	<i>aq a</i> : brain	<i>aq a</i> : proximal lateral rows (nerve cords?)
	<i>aq b</i> : digestive syncytium	<i>aq b</i> : scattered cells (neurons?)
	<i>aq c</i> : gut-wrapping cells, scattered cells (neurons?)	<i>aq c</i> : proximal lateral rows (nerve cords?)
	<i>aq e</i> : parenchymal cells	<i>aq d</i> : gut-wrapping cells
	<i>aq f</i> : gut-wrapping cells, scattered cells (neurons?)	<i>aq e</i> : anterior cells, scattered cells (neurons?)
	<i>aq g</i> : gut-wrapping cells, female gonads	<i>aq f</i> : gut-wrapping cells
	<i>slc1</i>	<i>slc1a</i> : brain
<i>slc1b</i> : male gonopore		
<i>slc1c</i> : brain, male gonopore		
<i>slc4</i>	<i>slc4a</i> : anterior cells	<i>slc4a</i> : gut-wrapping cells, mouth
	<i>slc4b</i> : brain, parenchymal cells	<i>slc4b</i> : nerve cords
	<i>slc4c</i> : anterior cells, parenchymal cells	<i>slc4c</i> : subepidermal cells, female gonads
<i>slc5</i>	<i>slc5a</i> : male gonopore	subepidermal cells, posterior lateral rows of cells
	<i>slc5b</i> : brain, parenchymal cells	

(Continued)

Table 1. (Continued)

	<i>I. pulchra</i>	<i>M. stichopi</i>
<i>slc8</i>	anterior cells	gut epithelium, mouth, posterior lateral rows of cells
<i>slc9</i>	mouth	proximal lateral rows (nerve cords?)
<i>slc12</i>	<i>slc12a</i> : brain, parenchymal cells	<i>slc12a</i> : male gonads, female gonads
	<i>slc12b</i> : brain, parenchymal cells	<i>slc12b</i> : male gonads
<i>slc13</i>	brain, parenchymal cells	<i>slc13b</i> : scattered cells (neurons?)
		<i>slc13c</i> : scattered cells (neurons?)
		<i>slc13d</i> : scattered cells (neurons?)
<i>slc26</i>	no expression revealed	<i>slc26a</i> : female gonads
		<i>slc26b</i> : gut-wrapping cells

Abbreviations: *amt*, ammonia transporter; *aq*, aquaporin; *ca*, carbonic anhydrase; *cd2ap*, CD2-associated protein; *hcn*, K⁺[NH₄⁺] channel; *pod*, podocin; *slc*, solute carrier transporter; *stom*, stomatin; *v-ATPase*, vacuolar H⁺-ATPase proton pump; *zo1*, zonula occludens 1

<https://doi.org/10.1371/journal.pbio.3000408.t001>

previous studies (summarized in [5,50]), and measured the ammonia excretion over 2 hours after bringing the animals into normal conditions. As expected, the ammonia excretion rates were strongly increased, in line with the short-term HEA-exposure experiments (Fig 2b). When we tested the expression level of excretion-related genes, we found that the expression of the passive ammonia transporters *rhesus* and three *amts*, as well as the active ammonia transporter *nka*, altered significantly (Fig 2c). Other differentially expressed genes were four *aquaporins*, the *v-ATPase*, and three *cas* (Fig 2c). These results indicate a putative role of these genes in ammonia excretion and suggest that acoels might not only excrete by diffusion and via passive transporters (*rhesus*, *amts*) but also by an alternative active transport mechanism (*nka*).

Inhibitor experiments support an active excretion mechanism via NKA transporter, as well as a passive vesicular transport mode, possibly mediated by Rhesus transporter

We further tested the involvement of NKA, V-ATPase A/B, and CA proteins in excretion, as well as a possible involvement of a vesicular transport mechanism, by conducting pharmacological inhibitor assays in *I. pulchra*, as previously demonstrated in other animals (summarized in [5,50]). Inhibition of the CA by acetazolamide did not show any significant change in ammonia excretion. Inhibition of the V-ATPase by concanamycin C seemed to lead to a decrease in ammonia excretion, although a 2-tailed *t* test did not support a significant change. In contrast, when perturbing the function of NKA with quabain, the ammonia excretion dropped significantly (Fig 2d), which further supports an active excretion mechanism via NKA, similar to what is described for many nephrozoans [10–12,14,17,19,20,25–27,31,51–53]. Interference with the vesicular transport using colchicine also led to a significant decrease in ammonia excretion, indicating a possible vesicular ammonia-trapping excretion mode (Fig 1c), as demonstrated in the midgut epithelium of the tobacco hornworm [26], the gills of the shore crab [27], and the integument of the nematode [14]. To test whether vesicular transport might occur through Rhesus transporter as shown in other studies (summarized in [5,50]), we revealed Rhesus protein localization by immunohistochemistry (Fig 2e). The protein localization mimicked the gene expression and revealed, apart from cells at the anterior tip and cells of the posterior epidermis, individual parenchymal cells affiliated with the digestive syncytium that extend ventrally. Higher magnification showed that the transporter was present in

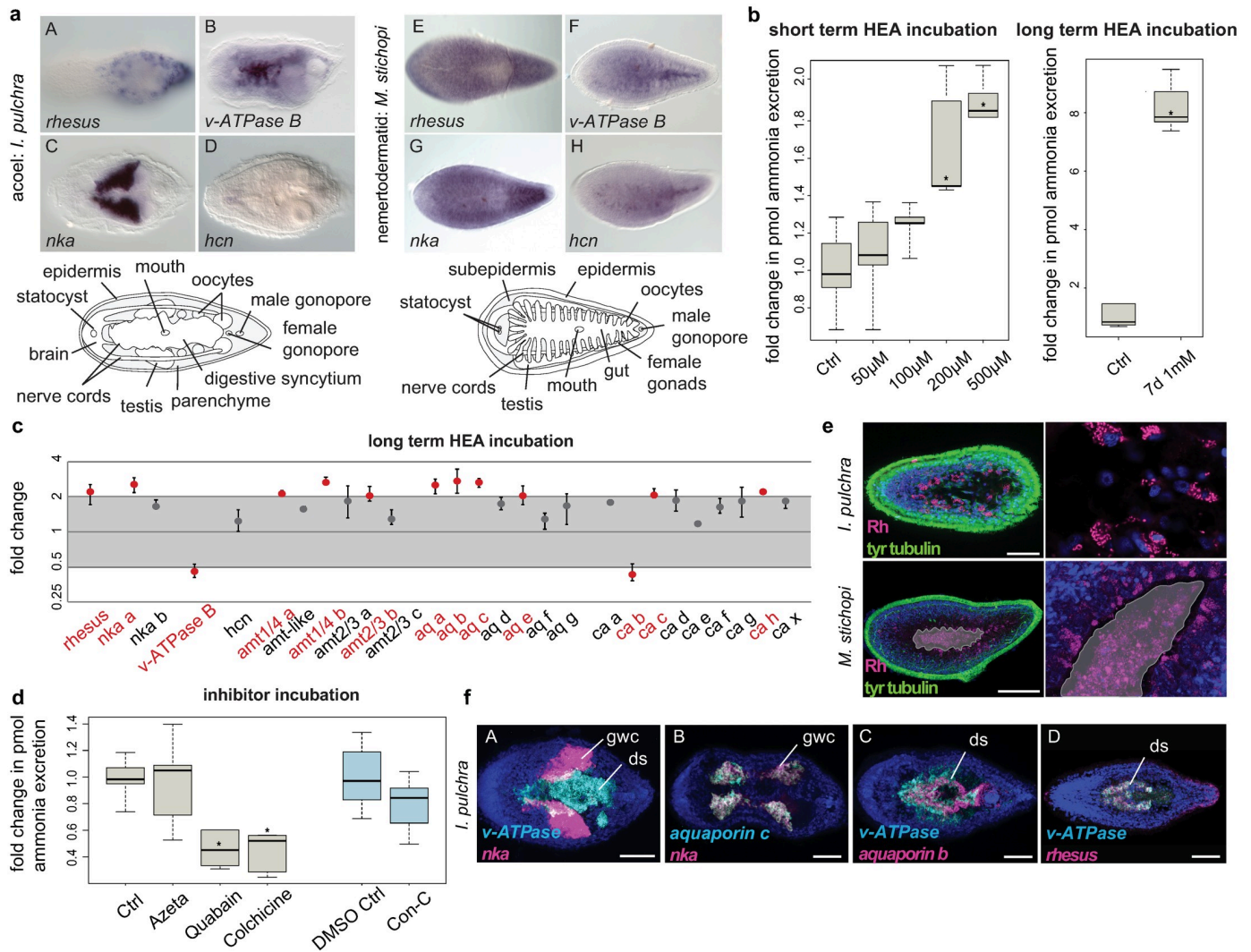


Fig 2. Excretion in acoelomorphs. (a) WMISH of *rhesus*, *v-ATPase*, *nka*, and *hcn* in *I. pulchra* and *M. stichopi*. (b) Ammonia excretion rates of *I. pulchra* before (Ctrl) and after exposure for 2 hours to 50, 100, 200, and 500 μM and after exposure for 7 days in 1 mM NH_4Cl (boxplot). Excretion was measured over 2 hours following the HEA treatments in at least three independent biological replicates, each divided into two separate samples (six measurements in total). Bold horizontal bars in boxes indicate the median; lower and upper box borders indicate lower and upper quartile; and whiskers indicate minimum and maximum. Asterisks label significant changes ($p < 0.02$ in an unpaired, 2-tailed t test with unequal variance). (c) Quantitative relative expression of *rhesus*, *nka*, *v-ATPase B*, *amts*, *aq*, and *ca* after 7 days of exposure in HEA (1 mM NH_4Cl). Each circle indicates the average of three independent biological replicates, each with four technical replicates. Error bars indicate minimum and maximum of the biological replicates (averaged technical replicates). A 1-fold change represents no change; ≥ 2 indicates significantly increased expression level; ≤ 0.5 indicates significantly decreased expression level (red labels). (d) Effects of different inhibitors on ammonia excretion rates in *I. pulchra* (boxplot, with illustration and replicates similar to Fig 2b). The concentrations used were 5 μM Con-C as a v-ATPase A/B inhibitor, 1 mM azetazolamide as an inhibitor of the CA, 1 mM quabain as an NKA inhibitor, and 2 mM colchicine for inhibiting the microtubule network. Con-C was diluted in 0.5% DMSO for which we used an appropriate Ctrl with 0.5% DMSO. (e) Protein localization of Rhesus in *I. pulchra* and *M. stichopi*. Syncytium and gut are indicated in gray, and the magenta staining of the lumen in *M. stichopi* is false-positive staining of the gut content. Fluorescent pictures are projections of merged confocal stacks. The nervous system is stained green with tyr tubulin. (f) Double fluorescent WMISH of *v-ATPase* and *nka*, *aq c* and *nka*, *v-ATPase* and *aq b*, and *v-ATPase* and *rhesus* in *I. pulchra*. White areas in the first panel are the result of merged stacks and not of overlapping expression. Nuclei are stained blue with DAPI. Anterior is to the left. Scale bars are 50 μm for *I. pulchra* and 100 μm for *M. stichopi*. Values underlying panels b and d are provided in S6 Table, and values underlying panel c are provided in S4 Table. amt, ammonia transporter; aq, aquaporin; CA, carbonic anhydrase; Con-C, concanamycin C; Ctrl, control; DAPI, 4',6-diamidino-2-phenylindole; ds, digestive syncytium; gwc, gut-wrapping cell; HCN, $\text{K}^+[\text{NH}_4^+]$ channel; HEA, high environmental ammonia; NKA, $\text{Na}^+/\text{K}^+[\text{NH}_4^+]$ ATPase; Rh, Rhesus glycoprotein; slc, solute carrier transporter; tyr, tyrosinated; v-ATPase, vacuolar H^+ -ATPase proton pump; WMISH, whole-mount in situ hybridization.

<https://doi.org/10.1371/journal.pbio.3000408.g002>

cytoplasmic vesicles and not on the cellular membrane (Fig 2e). This further indicated the presence of a vesicular transport mechanism, in which cellular ammonia moves via Rhesus transporters into vesicles and gets transferred to the membrane through the microtubule network [54] (Fig 1c). The antibody specificity was confirmed by an alignment of the epitope and the endogenous protein, as well as a western blot analysis (S6 Fig). Similar vesicular protein localization was also observed in *M. stichopi*, suggesting a similar cytoplasmic-vesicular role of Rhesus transporter in gut-affiliated cells, also in nemertodermatids (Fig 2e). These data further supported the involvement of NKA and Rhesus transporters in ammonia excretion and also indicated the presence of a putative vesicular transport mode in *I. pulchra*.

Double fluorescent whole-mount in situ hybridization of differentially expressed genes shows similar spatial arrangement in gut-associated domains in *I. pulchra* and *M. stichopi*

To obtain a better resolution and understanding of the relative topology of the differentially expressed genes, double fluorescent whole-mount in situ hybridization (WMISH) was conducted for *v-ATPase*, *nka*, *aquaporins b* and *c*, and *rhesus* (Fig 2f, S4 Fig). *Nka* and *v-ATPase* were expressed in a mutually exclusive manner, with *v-ATPase* to be restricted in the ventral region digestive syncytium and *nka* in an adjacent parenchymal, distal sac-shaped gut-wrapping domain (Fig 2fA, S4C Fig). The expression of *nka* was not extending to the male gonads (testes) (S4A Fig). *Aquaporin c* was coexpressed with *nka* (Fig 2fB), and *aquaporin b* was partially overlapping with *v-ATPase*, with *aquaporin b* expression extending into the posterior region of the digestive syncytium (Fig 2fC). Finally, *rhesus* was partly coexpressed with *v-ATPase* in the ventral region of the digestive syncytium (Fig 2fD). Similar coexpression analysis of the orthologous genes was also conducted for *M. stichopi* and revealed striking similarities in their spatial arrangement to *I. pulchra* (S4 and S7 Figs). *v-ATPase* expression was not overlapping with *nka*, as *v-ATPase* was restricted to the gut epithelium and in two proximal lateral rows of subepidermal cells, whereas *nka* was limited to cells lining the distal part of the epithelial branches of the gut extending toward the subepidermis (S4E and S7 Figs). *v-ATPase* was partly coexpressed with *rhesus* in ventral gut-affiliated cells (S7 Fig). Overall, these data revealed a similar spatial arrangement in gut-associated domains in both animals, which seems to be unrelated to the presence of an epithelial gut or a syncytium. However, given the fact that *I. pulchra* has a lumenless digestive tissue, ammonia is probably accumulated intracellularly in the syncytium before it gets expelled via the mouth, whereas in the case of *M. stichopi*, ammonia gets released in the gut lumen.

Taken together, our findings suggest that *I. pulchra* uses different mechanisms for ammonia excretion that are also known from nephrozoans; an active ammonia excretion mechanism via NKA through the digestive system, as suggested by in situ hybridization, and a passive vesicular transport mechanism likely mediated by Rhesus, through digestive and likely also epidermal tissues. Given the commonalities in the expression of the involved genes in both animals, these excretory mechanisms could be plesiomorphic for acoelomorphs.

HEA experiments suggest a diffusion mechanism also in the cnidarian *N. vectensis*

Because our results showed the involvement of active and passive transport mechanisms across digestive tissues outside Nephrozoa, we also investigated a non-bilaterian species, the cnidarian *N. vectensis* (S1b Fig), to test whether this excretion mode might also be present outside Bilateria. The only available excretion studies in cnidarians are few morphological studies, which suggested that the septa filaments of the anthozoan mesenteries and the radial canals of

medusozoans could serve as putative excretory sites [55], as well as some isotopic exchange experiments in *Hydra oligactis* that have shown that the gastrodermis seems to be involved in osmoregulation [56]. Moreover, there is evidence that Rh and AMT transporters are generally involved in ammonium excretion in corals [57], but localization studies that would suggest excretion sites are missing.

We first tested whether *N. vectensis* excretes via diffusion by exposing early-juvenile animals to HEA for 2 hours and measuring their ammonia excretion rates afterward, similar to the experiments performed with *I. pulchra*. We found that, also in *N. vectensis*, ammonia excretion increased significantly after HEA exposure starting at 200 and 500 μM NH_4Cl (Fig 3a). Measurements of the pH of each incubation medium showed that the pH dropped by 0.2 when the medium contained 500 μM NH_4Cl . However, when we measured the excretion of animals over 2 hours in a medium with an accordingly lowered pH, we found that a difference of 0.2 did not change the excretion rates (S2 Table). Therefore, the increase in ammonia excretion rates at 200 and 500 μM NH_4Cl indicates that ammonia excretion is concentration-dependent, supporting a diffusion mechanism also in *N. vectensis*.

Quantitative gene expression and inhibitor experiments indicates an involvement of passive but not active transport mechanisms in *N. vectensis*

We then exposed animals to 1 mM HEA for 7 days and tested the expression of the orthologous genes altered in *I. pulchra* treatments (*rh/amt*, *nka*, *v-ATPase B*, and *ca*) by qPCR. As expected from the short-term HEA-exposure experiment, specimens exposed for 7 days in the HEA condition showed increased ammonia excretion rates (Fig 3a). In contrast to *I. pulchra*, none of the two *nka* transporters showed a significant change in gene expression in animals exposed to HEA for 7 days (Fig 3b). However, the expression of the passive transporters *rhesus1*, *rhesus2*, *amt1/4b*, and *amt2/3e*, as well as *v-ATPase*, altered significantly (Fig 3b), indicating the putative involvement of these transporters in excretion of *N. vectensis*. To test whether Rhesus acts via a vesicular transport mechanism, we conducted the same pharmacological experiment as in *I. pulchra*. Contrary to the results from acoels, we found that inhibition of vesicular transport did not alter the ammonia excretion (Fig 3c). We also inhibited the excretory function of V-ATPase and CA proteins and found that none of them showed any significant change in ammonia excretion rates (Fig 3c). Finally, when we perturbed the function of NKA, the ammonia excretion rates did not alter (Fig 3c), confirming the qPCR results (Fig 3b) and further supporting the non-involvement of the NKA transporter in excretion. These results suggest that the ammonia excretion of *N. vectensis* is likely mediated by the passive Rhesus and AMT transporters, but neither relies on active transport mechanism mediated by NKA or on vesicular ammonia-trapping excretion mode.

Gene expression of excretion-related genes reveals the gastrodermis as excretory site in *N. vectensis*

To understand whether these genes were expressed in gastrodermal or epidermal cells, we revealed the spatial expression of *rhesus*, *amts*, *nka*, and *v-ATPase B* by WMISH in feeding primary polyps. All genes were mainly demarcating gastrodermal domains, such as the endodermal body wall, the directive mesenteries, septal filaments, and the pharynx (Fig 3d, S8 Fig). *Rhesus 1* was additionally expressed in the tentacular ectoderm (Fig 3dA). Protein localization of Rh, NKA, and V-ATPase B reflected the transcript expression patterns (Fig 3e, S9 Fig). High magnification of Rhesus antibody staining further revealed that the transporter was not expressed in cytoplasmic vesicles, supporting a non-vesicular transport mechanism, in agreement with the inhibitor experiments. Also, it showed that Rhesus was localized in individual

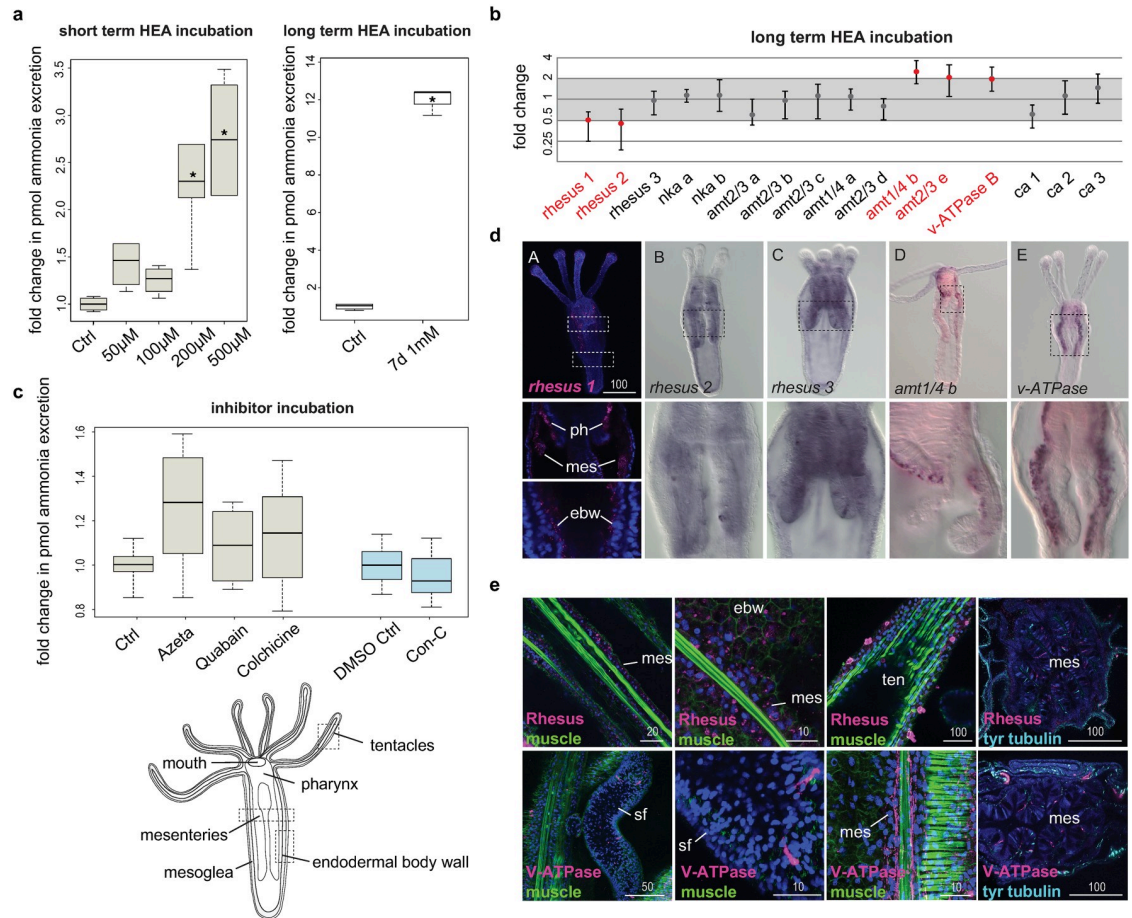


Fig 3. Excretion in *N. vectensis*. (a) Ammonia excretion rates of *N. vectensis* before (Ctrl) and after exposure for 2 hours to 50, 100, 200, and 500 μ M and after exposure for 7 days in 1mM NH_4Cl (boxplot). Excretion was measured over 2 hours following the HEA treatments in at least three independent biological replicates, each divided into two separate samples (six measurements in total). Bold horizontal bars in boxes indicate the median; lower and upper box borders indicate lower and upper quartile; and whiskers indicate minimum and maximum. Asterisks label significant changes. Significance, $p < 0.02$ (unpaired t test with unequal variance). (b) Quantitative relative expression of *rhesus*, *nka*, *v-ATPase B*, *amt*, and *ca* after exposure for 7 days in HEA (1 mM NH_4Cl). Each circle represents the average of five independent biological replicates, each with three technical replicates. A 1-fold change represents no change; ≥ 2 indicates increased expression level significantly; ≤ 0.5 indicates decreased expression level significantly (red labels). (c) Effects of different inhibitors on ammonia excretion rates in *N. vectensis* (boxplot, with illustration and replicates similar to Fig 2d). The concentrations used were 5–15 μ M Con-C as a V-ATPase A/B inhibitor, 1–3 mM acetazolamide as an inhibitor of the CA, 1–5 mM quabain as an NKA inhibitor, and 2–10 mM colchicine for inhibiting the microtubule network. Quabain was diluted in 0.5% DMSO, for which we used an appropriate Ctrl with 0.5% DMSO. $N = 3$ for all treatments. (d) Whole-mount in situ hybridization of *rh 1*, *rh 2*, *rh 3*, *v-ATPase*, and *amt1/4b* in feeding primary polyps. Anterior is to the top. (e) Protein localization of Rh and v-ATPase in *N. vectensis* early-juvenile polyps. The muscle filaments are labeled green with phalloidin, and the nervous system is stained cyan with tyr tubulin. Every picture is a full projection of merged confocal stacks. Nuclei are stained blue with DAPI. The regions shown are indicated with dashed boxes in the illustrated animal. Values underlying panels a and c are provided in S6 Table, and values underlying panel b are provided in S4 Table. amt, ammonia transporter; CA, carbonic anhydrase; Con-C, concanamycin C; Ctrl, control; DAPI, 4',6-diamidino-2-phenylindole; ebw, endodermal body wall; HEA, high environmental ammonia; mes, mesenteries; nka, $\text{Na}^+/\text{K}^+[\text{NH}_4^+]$ ATPase; ph, pharynx; rh, Rhesus glycoprotein; sf, septal filament; ten, tentacles; tyr, tyrosinated; v-ATPase, vacuolar H^+ -ATPase proton pump.

<https://doi.org/10.1371/journal.pbio.3000408.g003>

cells of the tentacular ectoderm with clumped structures at the tentacle surface, which resembled gland cells [58] (Fig 3e). The NKA antibody was localized in endodermal neurons and individual cells of the mesenteries, likely neural precursors (S9 Fig), thus suggesting a non-excretory function of this transporter, as indicated already from the qPCR and inhibitor

experiments. These data imply that gastrodermis-affiliated domains likely serve as excretory sites in *N. vectensis*.

Discussion

Overall, our findings show that acoelomorphs use, in addition to diffusion, active transport mechanisms, in contrast to what has been previously assumed for non-nephrozoans [1,39,40]. Our results also suggest that excretion takes place across digestive tissues and likely also across the epidermis, as indicated from the *rhesus* (both animals) and *amt* (only in *M. stichopi*) expression. *N. vectensis* also seem to use gastrodermal tissues as excretory sites, but we were not able to detect any active transport mechanism. However, we do not know whether the absence of active transport we find in *N. vectensis* is true for all cnidarians. It has been shown that differences in morphology and ecology (e.g., size and activity) are related with interspecific differences in excretion rates [59,60]. Therefore, bigger and more active cnidarian species might require more efficient modes of excretion, such as an active transport, in order to fulfill their metabolic requirements. Only more studies in other cnidarian species can elucidate this issue.

Digestive tissues with additional or assigned excretory roles have also been reported in several nephrozoans (e.g., vertebrates, annelids, insects, nematodes, tunicates, chaetognaths) [16,26,31,61–67]. In the light of our results, this excretion mechanism likely reflects an ancient mechanism, before the evolution of specialized organs, such as nephridia (S10 Fig). The molecular spatial arrangement of the excretion sites in non-nephrozoans, however, is not sharing topological arrangements with common nephridial domains of nephrozoans (Fig 1b), suggesting that they are evolutionarily unrelated to nephridia. It still remains unclear whether these domains are multifunctional or consist of specialized excretory subdomains; however, a degree of cell subfunctionalization seems to be present, as indicated by the localized gene expression in different groups of gut-wrapping and gut epithelial cells. We can, however, exclude the presence of ultrafiltration sites, in agreement with previous ultrastructure studies in acoelomorphs [68], because the homologous essential molecular components of the ultrafiltration sites of nephridia and nephrocytes are mostly expressed in neural domains in acoelomorphs and are absent in non-bilaterians (nephrens), suggesting their later recruitment in the nephrozoan filtration apparatus (Fig 4).

Recently, a new study was published suggesting the non-monophyly of Deuterostomia and a placement of Ambulacraria (Echinodermata + Hemichordata) as the sister group of Nematodermatida + (Acoela + *Xenoturbella*) [69]. If true, this novel topology has vast consequences for our understanding of the evolution of all major bilaterian organ systems including the excretory organs [70]. Based on this phylogeny, either excretory organs have been independently evolved in Ambulacraria and (Chordata + Protostomia) or they have been already present in the last common ancestor of Bilateria and got lost secondarily in nemertodermatids, acoels, and *Xenoturbella*. Ambulacraria possesses a metanephridial type of excretory organ, which, according to some authors, is independently evolved [43,71]; therefore, excretory organs of Ambulacraria, Chordata, and Protostomia might not be homologous. In the scenario of the presence of an excretory organ in the last common ancestor of Bilateria, one would have to assume a complete reduction of excretory organs in the lineage to Nematodermatida + (Acoela + *Xenoturbella*) without morphological or molecular traces. However, the support values for the main branches of Bilateria in the [69] study are low, and the study also does not recover the Xenacoelomorpha as clade. In-depth analyses are necessary to test whether the new topology is not an artifact that is based on the new approach the study uses for the phylogenomic analyses.

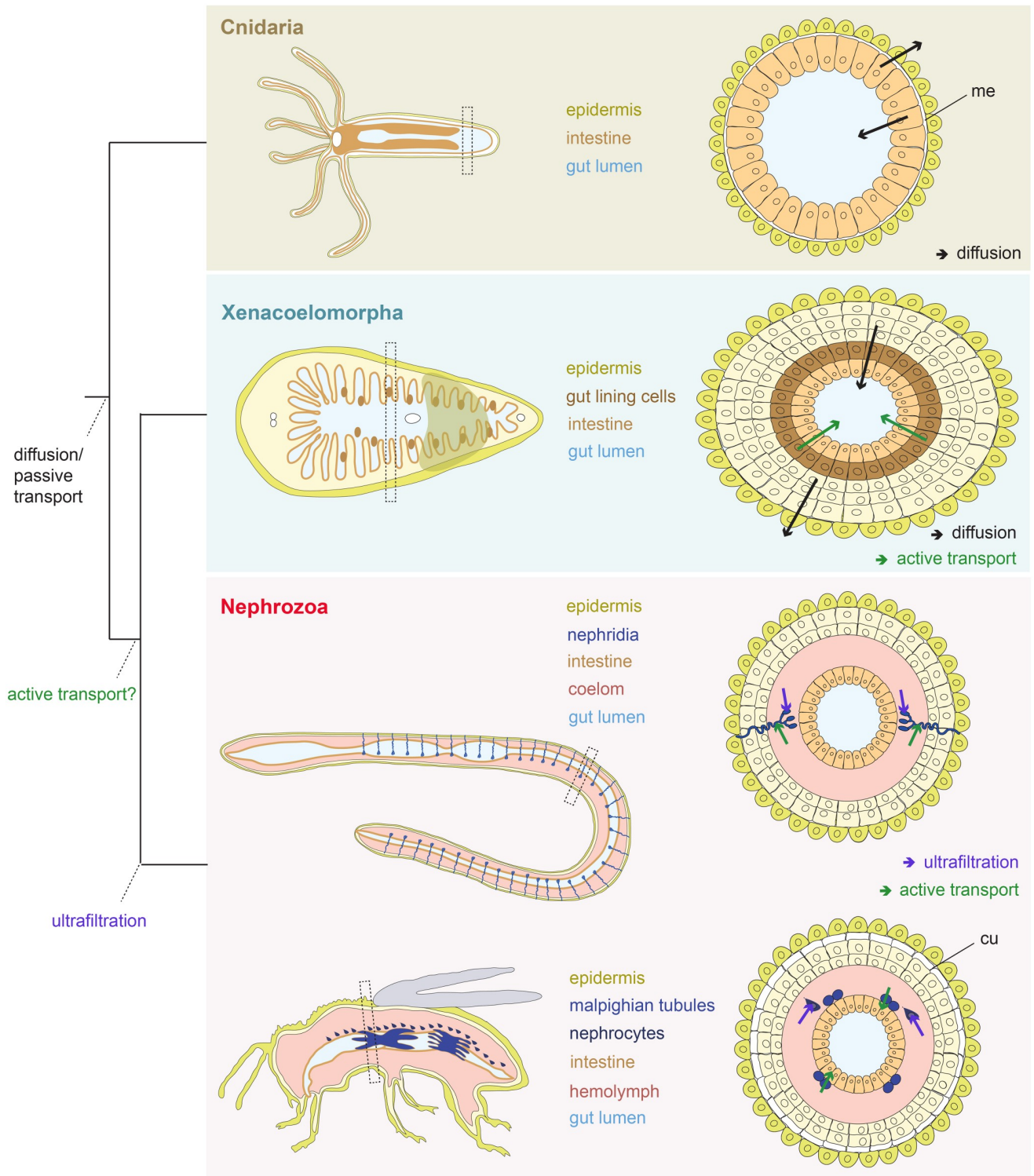


Fig 4. Evolution of excretory mechanisms. Illustration of the proposed direction of fluxes in Cnidaria and Xenacoelomorpha and evolution of active ammonia transport and ultrafiltration mechanisms. Cnidaria (e.g., *N. vectensis*) excrete across their intestinal epithelium (and probably across the epidermis too) via diffusion, whereas in xenacoelomorphs, excretion occurs both via diffusion across the epidermis and gut-associated tissues and via active transport across gut-associated tissues. Ultrafiltration mechanism originated within Nephrozoa. cu, cuticle; me, mesoglea.

<https://doi.org/10.1371/journal.pbio.3000408.g004>

To conclude, our study shows that active transport mechanism and excretion through digestive tissues predates the evolution of specialized excretory systems. Whether this is based on a convergent recruitment or reflects an ancestral state for Bilateria remains unclear. However, if the latter is true, it correlates with the emergence of multilayered body plans and solid internal parenchymes that separate the body wall from their digestive tract, as seen in xenacoelomorphs and nephrozoans. We thus propose that diffusion mechanisms were the major excretory modes present in animals with single-layered epithelial organization (Fig 4). The emergence of more complex, multilayered body plan necessitated an active transport of excreted, which was later recruited in specific compartments of the complex excretory organs in the lineage of Nephrozoa.

Methods

No statistical methods were used to predetermine sample size. The experiments were not randomized. The investigators were not blinded to allocation during experiments and outcome assessment.

Gene cloning and orthology assignment

Putative orthologous sequences of genes of interest were identified by tBLASTx search against the transcriptome (SRR2681926) of *I. pulchra*, the transcriptome (SRR2681155) and draft genome of *M. stichopi*, and the genome of *N. vectensis* (<http://genome.jgi.doe.gov>). Additional transcriptomes of Xenacoelomorpha species investigated were as follows: *Childia submaculatum* (Acoela) (SRX1534054), *Convolutriloba macropyga* (Acoela) (SRX1343815), *Diopisthoporus gymnopharyngeus* (Acoela) (SRX1534055), *Diopisthoporus longitubus* (Acoela) (SRX1534056), *Eumecynostomum macrobursalium* (Acoela) (SRX1534057), *Hofstenia miamia* (Acoela) (PRJNA241459), *Ascoparia* sp. (Nemertodermatida) (SRX1343822), *Nemertoderma westbladi* (Nemertodermatida) (SRX1343819), *Sterreria* sp. (Nemertodermatida) (SRX1343821), *Xenoturbella bocki* (*Xenoturbella*) (SRX1343818), and *Xenoturbella profunda* (*Xenoturbella*) (SRP064117). Data were deposited in the Dryad repository: <https://doi.org/10.5061/dryad.bq068jr> [72].

Sequences for the placozoan *Trichoplax adhaerens*, the sponge *Amphimedon queenslandica*, the ctenophore *Mnemiopsis leidy*, the protist *Capsaspora owczarzaki*, the amoeba *Dictyostelium discoideum*, and the nephrozoans *Homo sapiens*, *Saccoglossus kowalevskii*, *Strongylocentrotus purpuratus*, *Xenopus laevis*, *Branchiostoma lanceolatum*, *Capitella teleta*, *Crassostrea gigas*, *Lotia gigantea*, *Schmidtea mediterranea*, *Tribolium castaneum*, *Caenorhabditis elegans*, and *Drosophila melanogaster* were obtained from Uniprot and NCBI public databases. Gene orthology of genes of interest identified by tBLASTx was tested by reciprocal BLAST against NCBI Genbank and followed by phylogenetic analyses. Amino acid alignments were made with MUSCLE [73]. RAxML (version 8.2.9) [74] was used to conduct a maximum-likelihood phylogenetic analysis. Fragments of the genes of interest were amplified from cDNA of *I. pulchra*, *M. stichopi*, and *N. vectensis* by PCR using gene-specific primers. PCR products were purified and cloned into a pGEM-T Easy vector (Promega, Madison, WI, USA) according to the manufacturer's instructions, and the identity of inserts was confirmed by sequencing. Gene accession numbers of the gene sequences are listed in the S3 Table.

Animal systems

Adult specimens of *I. pulchra* (Smith & Bush, 1991), *M. stichopi* Westblad, 1949, and *N. vectensis* Stephenson, 1935 were kept and handled as previously described [75–78].

WMISH

Animals were manually collected, fixed, and processed for in situ hybridization as described [79,80]. Labeled antisense RNA probes were transcribed from linearized DNA using digoxigenin-11-UTP (Roche, Basel, Switzerland) or labeled with DNP (Mirus Bio, Madison, WI, USA) according to the manufacturer's instructions. For *I. pulchra* and *M. stichopi*, colorimetric WMISH was performed according to the protocol outlined in [79]. For *N. vectensis*, we followed the protocol described by [81]. Double fluorescent in situ hybridization (FISH) was performed as the colorimetric WMISH with the following modifications: after the posthybridization steps, animals were incubated overnight with peroxidase-conjugated antibodies at 4 °C (anti-DIG-POD [Roche, Basel, Switzerland], 1:500 dilution, and anti-DNP [Perkin Elmer, Waltham, MA, USA], 1:200 dilution) followed by the amplification of the signal with fluorophore-conjugated tyramides (1:100 TSA reagent diluents [Perkin Elmer, Waltham, MA, USA] TSA Plus Cy3 or Cy5 Kit). Residual enzyme activity was inhibited via 45-minute incubation in 0.1% hydrogen peroxide in PTW followed by four PTW washes prior to addition and development of the second peroxidase-conjugated antibody [82].

Whole-mount immunohistochemistry

Animals were collected manually, fixed in 4% paraformaldehyde in SW for 50 minutes, washed 3 times in PBT, and incubated in 4% sheep serum in PBT for 30 minutes. The animals were then incubated with commercially available primary antibodies (anti-RhAG [ab55911] rabbit polyclonal antibody, dilution 1:50 [Abcam, Cambridge, UK], anti-Na⁺/K⁺ ATPase α 1 subunit rat monoclonal antibody, dilution 1:100 [Sigma-Aldrich, St. Louis, MO, USA], and anti-V-ATPase B1/2 [L-20] goat polyclonal antibody, dilution 1:50 [Santa Cruz Biotechnology, Dallas, TX, USA]) overnight at 4 °C, washed 5 times in PBT, and followed by incubation in 4% sheep serum in PBT for 30 minutes. Specimens were then incubated with a secondary antibody (anti-rabbit-AlexaFluor 555 [Invitrogen, Carlsbad, CA, USA] or anti-rat-AlexaFluor 555 and anti-goat-AlexaFluor 555) diluted 1:1,000 overnight at 4 °C followed by 10 washes in PBT. Nuclei were stained by incubation of animals in DAPI 1:1,000, and f-actin was stained by incubation in BODIPY-labeled phalloidin (5 U/ml) overnight.

Inhibitor and HEA experiments

For excretion experiments, approximately 300 *I. pulchra* (the number varied slightly between the biological replica but was similar in the corresponding controls and treatments) and 10 *N. vectensis* were placed into glass vials with 2 ml UV-sterilized natural seawater (1:4 diluted with distilled water for *N. vectensis*) containing the appropriate inhibitor or ammonia concentration. Animals were given 10 minutes to adjust to the medium before the solution was exchanged with 2 ml of fresh medium with the same appropriate condition. For the inhibitor experiment, the medium was removed after 2 hours and stored at -80 °C for later measurements. Animals from the short-term HEA experiments were incubated for 2 hours, rinsed five times over 20–30 minutes, and incubated for another 2 hours in fresh medium without additional ammonia, after which the medium was removed and frozen at -80 °C. We tested different inhibitor concentrations that were used in previous studies in other invertebrates [10,12,14,19,27]. The concentrations of 5–15 μ M concanamycin C for inhibiting V-ATPase A/B, 1–3 mM acetazolamide as an inhibitor of the CA, 1–5 mM quabain to inhibit the NKA, and 2–10 mM colchicine for inhibiting the microtubule network were selected, as no other effects like shrinking or obvious changes in morphology or behavior were observed. After the inhibitor incubations, the animals were washed several times and monitored in normal conditions for several days to ensure that the inhibitors did not cause any unspecific permanent effects.

Concanamycin C was diluted in DMSO with a final concentration of 0.5% DMSO per sample, for which we used an appropriate control with 0.5% DMSO. For the HEA experiments, we enriched seawater with NH_4Cl to the final ammonia concentrations of 50 μM , 100 μM , 200 μM , 500 μM , and 1 mM. We also measured the pH of both incubation mediums (HEA and control), and we found no difference. All experiments were independently repeated at least three times at different time points, and each repeat was divided into two samples. The values are provided in [S6 Table](#).

Determination of ammonia excretion

Ammonia concentrations were measured with an ammonia-sensitive electrode (Orion, Thermo Scientific, Waltham, MA, USA) according to [52]. Samples were diluted 1:4 with distilled water to prevent salt precipitation (900 μl sample + 2.7 ml water), and total ammonia was transformed into gaseous NH_3 by adding 54 μl ionic strength adjusting solution (1.36 ml/l trisodiumcitrate dihydrate, 1 M NaOH). Because of the small ammonia concentrations, the electrode-filling solution was diluted to 10% with distilled water, as suggested in the electrode manual. In control conditions, we determined an average excretion of 44 pmol per adult animal per hour, although the excretion varied between different biological replicates from different generations (minimum 32 pmol/animal/hour, maximum 52 pmol/animal/hour), possibly because of slightly fluctuating conditions during long-term animal rearing. Solutions with defined concentrations of NH_4Cl for the standard curves were made together with the solutions used in the experiments and stored in a similar way at -80°C . The differences in excretion rates were tested for significance with an unpaired, 2-tailed t test with unequal variance, and a p -value < 0.02 was seen as significant. Boxplots were created with “R.”

Quantitative gene expression

In total, 100 treated *I. pulchra* and 5 *N. vectensis* were collected after 7 days of incubation in HEA conditions (1 mM NH_4Cl) and tested for quantitative gene expression using the BIORAD CFX96 (Bio-Rad, Hercules, CA, USA) Real-time PCR detection system. ddCt values were calculated between treated and control animals and converted to fold differences. All experiments were repeated three to five times with different specimens (three biological replicates for *I. pulchra* and five biological replicates for *N. vectensis*), and two to four technical replicates were tested for each biological replicate (four biological replicates for *I. pulchra* and three biological replicates for *N. vectensis*). Fold changes were calculated using polyubiquitin, actin, and 18S as references for *I. pulchra* and *ATPsynthase* and *EF1b* as references for *N. vectensis* [83], and a threshold of 2-fold difference was chosen as a significant change. The Ct values are provided in [S4 Table](#), and the primer sequences used are provided in [S5 Table](#).

Western blot

Whole-animal extracts (50 *I. pulchra* adults and 5 *N. vectensis* juveniles) were fractionated by SDS-PAGE, loaded on Mini-PROTEAN TGX Stain-Free Precast Gels (Bio-Rad, Hercules, CA, USA), and transferred to a nitrocellulose membrane using a transfer apparatus according to the manufacturer's protocols (Bio-Rad, Hercules, CA, USA). After incubation with 5% nonfat milk in TBST (10 mM Tris, [pH 8.0], 150 mM NaCl, 0.5% Tween 20) for 60 minutes, the membrane was washed once with TBST and incubated with antibodies against Rhesus (1:1,000) and NKA (1:500) at 4°C for 12 hours. Membranes were washed three times for 10 minutes and incubated with a 1:5,000 dilution of horseradish peroxidase-conjugated anti-mouse or anti-rabbit antibodies for 2 hours. Blots were washed with TBST three times and developed with

the ECL system (Amersham Biosciences, Little Chalfont, UK) according to the manufacturer's protocols.

Documentation

Colorimetric WMISH specimens were imaged with a Zeiss AxioCam HRc mounted on a Zeiss Axioscope A1 equipped with Nomarski optics and processed through Photoshop CS6 (Adobe, San Jose, CA, USA). Fluorescent-labeled specimens were analyzed with a Leica SP5 confocal laser microscope (Leica Microsystems, Wetzlar, Germany) and processed by the Fiji software version 2.0.0-rc-42/1.50d [84]. Figure plates were arranged with Illustrator CS6 (Adobe, San Jose, CA, USA). Data were deposited in the Dryad repository: <https://doi.org/10.5061/dryad.bq068jr> [72].

Supporting information

S1 Fig. Excretion-related gene complement in different animal lineages and outgroups and animals in this study. (a) Transcriptome and genome mining of excretion-related gene repertoire in *I. pulchra*, *H. miamia*, *C. macropyga*, *D. longitubus*, *D. gymnopharyngeus*, *E. macrobursalium*, and *C. submaculatum* as representatives of Acoela; *Sterreria* sp., *Ascoparia* sp., *M. stichopi*, and *N. westbladi* as representatives of Nemertodermatida; *X. bocki* and *X. profunda* as representatives of *Xenoturbella*; *N. vectensis* as a representative of cnidarians; *T. adhaerens* as a representative of placozoans; *A. queenslandica* as a representative of sponges; and the deuterostomes *H. sapiens*, *S. kowalevskii*, *S. purpuratus*, *X. laevis*, and *B. lanceolatum* and protostomes *C. teleta*, *C. gigas*, *L. gigantea*, *S. mediterranea*, *T. castaneum*, *C. elegans*, and *D. melanogaster* as representatives of Nephrozoa. Data are based on this study unless stated otherwise. (b) Pictures of the acoelomorph representatives *I. pulchra* (scale bar = 50 μ m) and *M. stichopi* (scale bar = 100 μ m) and the cnidarian representative *N. vectensis* (scale bar = 2 mm). Animal illustrations are taken from phylopic.org.

(TIF)

S2 Fig. Orthology analysis. Putative orthologous sequences of genes of interest were identified by tBLASTx search against the transcriptome (SRR2681926) of *I. pulchra*, the transcriptome (SRR2681155) and draft genome of *M. stichopi*, and the genome of *N. vectensis* (<http://genome.jgi.doe.gov>). Additional transcriptomes of Xenacoelomorpha species investigated were as follows: *C. submaculatum* (Acoela) (SRX1534054), *C. macropyga* (Acoela) (SRX1343815), *D. gymnopharyngeus* (Acoela) (SRX1534055), *D. longitubus* (Acoela) (SRX1534056), *E. macrobursalium* (Acoela) (SRX1534057), *H. miamia* (Acoela) (PRJNA241459), *Ascoparia* sp. (Nemertodermatida) (SRX1343822), *N. westbladi* (Nemertodermatida) (SRX1343819), *Sterreria* sp. (Nemertodermatida) (SRX1343821), *X. bocki* (Xenoturbella) (SRX1343818), and *X. profunda* (Xenoturbella) (SRP064117). Bayesian phylogenetic analysis is supporting orthology for genes investigated in this study. Red color refers to Xenacoelomorpha taxa, and blue color refers to *N. vectensis*. Bootstrap values are shown when equal or above 20%. Branches crossed by a double slash were shortened to make figures' plates more compact. Names of genes or proteins, if available, follow the name of organism(s); otherwise, the accession number is written. Asterisks indicate genes with a spatial expression by WMISH. WMISH, whole-mount in situ hybridization.

(PDF)

S3 Fig. WMISH of ultrafiltration and tubule and duct-related genes in *I. pulchra* and *M. stichopi*. Expression of genes encoding the slit diaphragm components related to ultrafiltration *nephrin/kirre*, *cd2ap*, *zo1*, and *stomatin/podocin*, and the SLCs related to excrete modification

slc1, *slc5*, and *slc13* (proximal tubule) and *slc4*, *slc8*, *slc9*, *slc12*, and *slc26* (distal tubule and duct) in *I. pulchra* and *M. stichopi*. The inset in panel A3 shows a different focal plane of the indicated domain and in panel E3 shows a different focal plane of the animal. The columns next to *M. stichopi* panels show higher magnifications of the indicated domains. Anterior is to the left. BG indicates background staining. BG, background; *cd2ap*, CD2-associated protein; mo, mouth; mg, male gonopore; SLC, solute carrier transporter; st, statocyst; WMISH, whole-mount in situ hybridization; *zol*, zonula occludens 1.
(TIF)

S4 Fig. Double fluorescent WMISH of excretion-related components and molecular markers of digestive, nervous, and reproductive systems in *I. pulchra* and *M. stichopi*. Coexpression analysis of *nka* with the reproductive system markers *piwi* and *vasa* (A), *hcn* with the nervous system marker *chaT* (B), *v-ATPase* with the digestive marker *plastin* in *I. pulchra* (C), *slc4b* with the nervous system marker tyrosinated tubulin (D), and *v-ATPase* with the digestive marker *plastin* in *M. stichopi* (E). Every picture is a full projection of merged confocal stacks. Nuclei are stained blue with DAPI. Anterior is to the left. Scale bars are 50 μm for *I. pulchra* and 100 μm for *M. stichopi*. br, brain; *chaT*, choline acetyltransferase; DAPI, 4',6-diamidino-2-phenylindole; ds, digestive syncytium; gwc, gut-wrapping cell; *hcn*, $\text{K}^+[\text{NH}_4^+]$ channel; nc, nerve cord; *nka*, $\text{Na}^+/\text{K}^+[\text{NH}_4^+]$ ATPase; *slc*, solute carrier transporter; te, testis; *v-ATPase*, vacuolar H^+ -ATPase proton pump; WMISH, whole-mount in situ hybridization.
(TIF)

S5 Fig. WMISH of the ammonia excretion-related genes *rh*, *v-ATPase B*, *nka*, *ca*, *hcn*, *amts*, and *aquaporins* in *I. pulchra* and *M. stichopi*. The insets in panels B6, C1, and C3 show different focal planes of the animals. The columns next to *M. stichopi* panels show higher magnifications of the indicated domains, except of G2', which shows a different focal plane of the animal. The inset in panel G5' shows a side view of the animal. Anterior is to the left. *amt*, ammonia transporter; *ca*, carbonic anhydrase; mo, mouth; *nka*, $\text{Na}^+/\text{K}^+[\text{NH}_4^+]$ ATPase; *rh*, Rhesus glycoprotein; *v-ATPase*, vacuolar H^+ -ATPase proton pump; WMISH, whole-mount in situ hybridization.
(TIF)

S6 Fig. Western blot of Rhesus in *I. pulchra* and Rhesus and NKA in *N. vectensis*. Below each blot, the sequence alignment of the endogenous protein and the antigen is provided, highlighted in pink. NKA, $\text{Na}^+/\text{K}^+[\text{NH}_4^+]$ ATPase.
(PDF)

S7 Fig. Double fluorescent WMISH of *v-ATPase* with *nka* and *v-ATPase* with *rhesus* in *M. stichopi*. Every picture is a full projection of merged confocal stacks. Nuclei are stained blue with DAPI. Anterior is to the left. DAPI, 4',6-diamidino-2-phenylindole; dlr, distal lateral row; ds, digestive syncytium; gwc, gut-wrapping cell; *nka*, $\text{Na}^+/\text{K}^+[\text{NH}_4^+]$ ATPase; *v-ATPase*, vacuolar H^+ -ATPase proton pump; WMISH, whole-mount in situ hybridization.
(TIF)

S8 Fig. WMISH of ammonia transporters in *N. vectensis*. Gene expression of *amt2/3a*, *amt2/3b*, *amt2/3c*, *amt2/3d*, and *amt1/4a* in juvenile polyps. Anterior is to the left. *amt*, ammonia transporter; WMISH, whole-mount in situ hybridization.
(TIF)

S9 Fig. WMISH and protein localization of NKA in *N. vectensis*. Gene expression of *nka a* and *nka b* in juvenile polyps. Anterior is to the left. Protein localization of NKA in *N. vectensis* juvenile polyps. The muscle filaments are labeled green with phalloidin, and the nervous

system is stained cyan with tyrosinated tubulin. Every picture is a full projection of merged confocal stacks. Nuclei are stained blue with DAPI. The regions shown are indicated with dashed boxes in the illustrated animal. DAPI, 4',6-diamidino-2-phenylindole; ebw, endodermal body wall; mes, mesenteries; n, neuron; NKA, $\text{Na}^+/\text{K}^+[\text{NH}_4^+]$ ATPase; sf, septal filament; WMISH, whole-mount in situ hybridization.

(TIF)

S10 Fig. Phylogenetic tree showing the relationship of animal groups in which the role of gut in excretion has been demonstrated or proposed.

(TIF)

S1 Table. Compilation of excretion-related gene expression/role data for metazoan and nonmetazoan taxa for genes investigated in this study, when data are available. Data are based on this study unless stated otherwise. Question marks represent missing data.

(PDF)

S2 Table. *N. vectensis* excretion in different pH.

(PDF)

S3 Table. Accession numbers and transcript numbers from Xenacoelomorph transcripts used in S1 and S2 Figs.

(PDF)

S4 Table. QPCR raw data. QPCR, quantitative PCR.

(PDF)

S5 Table. QPCR primers used in this study. QPCR, quantitative PCR.

(PDF)

S6 Table. Ammonia excretion measurements raw data.

(PDF)

Acknowledgments

We thank Fabian Rentzsch, Patrick Steinmetz, and Hanna Kraus (Sars Centre, University of Bergen, Norway) for providing *N. vectensis* animals and cDNA. Peter Ladurner provided the *I. pulchra* cultures that were kept in the animal facility at the Sars Centre. We thank all S9 lab members for the help with the collections of *M. stichopi*.

Author Contributions

Conceptualization: Carmen Andrikou, Andreas Hejnlol.

Formal analysis: Carmen Andrikou, Daniel Thiel, Juan A. Ruiz-Santesteban.

Funding acquisition: Juan A. Ruiz-Santesteban, Andreas Hejnlol.

Investigation: Carmen Andrikou, Daniel Thiel, Juan A. Ruiz-Santesteban, Andreas Hejnlol.

Methodology: Carmen Andrikou, Daniel Thiel.

Project administration: Andreas Hejnlol.

Resources: Carmen Andrikou.

Supervision: Carmen Andrikou.

Validation: Daniel Thiel.

Visualization: Carmen Andrikou, Andreas Hejnl.

Writing – original draft: Carmen Andrikou, Andreas Hejnl.

Writing – review & editing: Carmen Andrikou, Daniel Thiel, Juan A. Ruiz-Santesteban.

References

- Schmidt-Rhaesa A. The evolution of organ systems. New York: Oxford University Press; 2007.
- Jondelius U, Ruiz-Trillo I, Baguña J, Riutort M. The Nemertodermatida are basal bilaterians and not members of the Platyhelminthes. *Zool Scr.* 2002; 31(2):201–15.
- Ichimura K, Sakai T. Evolutionary morphology of podocytes and primary urine-producing apparatus. *Anat Sci Int.* 2017; 92(2):161–72. <https://doi.org/10.1007/s12565-015-0317-7> PMID: 26627098
- Ruppert EE, Smith PR. The functional-organization of filtration nephridia. *Biol Rev.* 1988; 63(2):231–58.
- Larsen EH, Deaton LE, Onken H, O'Donnell M, Grosell M, Dantzler WH, et al. Osmoregulation and Excretion. *Compr Physiol.* 2014; 4(2):405–573. <https://doi.org/10.1002/cphy.c130004> PMID: 24715560
- Locke M, Russell VW. Pericardial cells or athrocytes. In: Harrison FW, Locke M, editors. *Microscopic Anatomy of Invertebrates*. 11B:Insecta. New York: Wiley-Liss; 1998. p. 687–709.
- Kokkinopoulou M, Guler MA, Lieb B, Barbeck M, Ghanaati S, Markl J. 3D-ultrastructure, functions and stress responses of gastropod (*Biomphalaria glabrata*) rhogocytes. *PLoS ONE.* 2014; 9(6):e101078. <https://doi.org/10.1371/journal.pone.0101078> PMID: 24971744
- Wessing A, Eichelberg D. Ultrastructural aspects of transport and accumulation of substances in the malpighian tubules. *Fortschr Zoologie.* 1975; 23:148–72.
- Adlimoghaddam A, Weihrauch D, O'Donnell MJ. Localization of K(+), H(+), Na(+) and Ca(2)(+) fluxes to the excretory pore in *Caenorhabditis elegans*: application of scanning ion-selective microelectrodes. *J Exp Biol.* 2014; 217(Pt 23):4119–22. <https://doi.org/10.1242/jeb.112441> PMID: 25278475
- Thiel D, Hugenschutt M, Meyer H, Paululat A, Quijada-Rodriguez AR, Purschke G, et al. Ammonia excretion in the marine polychaete *Eurythoe complanata* (Annelida). *J Exp Biol.* 2016; 220(Pt 3):425–36. <https://doi.org/10.1242/jeb.145615> PMID: 27852754
- Weihrauch D, Wilkie MP, Walsh PJ. Ammonia and urea transporters in gills of fish and aquatic crustaceans. *J Exp Biol.* 2009; 212(Pt 11):1716–30. <https://doi.org/10.1242/jeb.024851> PMID: 19448081
- Weihrauch D, Chan AC, Meyer H, Doring C, Sourial M, O'Donnell MJ. Ammonia excretion in the freshwater planarian *Schmidtea mediterranea*. *J Exp Biol.* 2012; 215(Pt 18):3242–53. <https://doi.org/10.1242/jeb.067942> PMID: 22660782
- Cannon JT, Vellutini BC, Smith J 3rd, Ronquist F, Jondelius U, Hejnl A. Xenacoelomorpha is the sister group to Nephrozoa. *Nature.* 2016; 530(7588):89–93. <https://doi.org/10.1038/nature16520> PMID: 26842059
- Adlimoghaddam A, Boeckstaens M, Marini AM, Treberg JR, Brassinga AKC, Weihrauch D. Ammonia excretion in *Caenorhabditis elegans*: mechanism and evidence of ammonia transport of the Rhesus protein CeRhr-1. *J Exp Biol.* 2015; 218(5):675–83.
- Adlimoghaddam A, O'Donnell MJ, Kormish J, Banh S, Treberg JR, Merz D, et al. Ammonia excretion in *Caenorhabditis elegans*: Physiological and molecular characterization of the *rhr-2* knock-out mutant. *Comp Biochem Physiol A.* 2016; 195:46–54.
- Blaesse AK, Broehan G, Meyer H, Merzendorfer H, Weihrauch D. Ammonia uptake in *Manduca sexta* midgut is mediated by an amiloride sensitive cation/proton exchanger: Transport studies and mRNA expression analysis of NHE7, 9, NHE8, and V-ATPase (subunit D). *Comp Biochem Phys A.* 2010; 157(4):364–76.
- Cruz MJ, Sourial MM, Treberg JR, Fehsenfeld S, Adlimoghaddam A, Weihrauch D. Cutaneous nitrogen excretion in the African clawed frog *Xenopus laevis*: effects of high environmental ammonia (HEA). *Aquatic toxicology.* 2013; 136–137:1–12. <https://doi.org/10.1016/j.aquatox.2013.03.002> PMID: 23624175
- Fehsenfeld S, Weihrauch D. The role of an ancestral hyperpolarization-activated cyclic nucleotide-gated K⁺ channel in branchial acid-base regulation in the green crab, *Carcinus maenas*. *J Exp Biol.* 2016; 219(Pt 6):887–96. <https://doi.org/10.1242/jeb.134502> PMID: 26787479
- Gerber L, Lee CE, Grousset E, Blondeau-Bidet E, Boucheker NB, Lorin-Nebel C, et al. The Legs Have It: In Situ Expression of Ion Transporters V-Type H(+)-ATPase and Na(+)/K(+)-ATPase in the Osmoregulatory Leg Organs of the Invading Copepod *Eurytemora affinis*. *Physiol Biochem Zool.* 2016; 89(3):233–50. <https://doi.org/10.1086/686323> PMID: 27153133

20. Hu MY, Lee JR, Lin LY, Shih TH, Stumpp M, Lee MF, et al. Development in a naturally acidified environment: Na⁺/H⁺-exchanger 3-based proton secretion leads to CO₂ tolerance in cephalopod embryos. *Front Zool.* 2013; 10(1):51. <https://doi.org/10.1186/1742-9994-10-51> PMID: 23988184
21. Mak DO, Dang B, Weiner ID, Foskett JK, Westhoff CM. Characterization of ammonia transport by the kidney Rh glycoproteins RhBG and RhCG. *Am J Physiol Renal Physiol.* 2006; 290(2):F297–305. <https://doi.org/10.1152/ajprenal.00147.2005> PMID: 16131648
22. Patrick ML, Aimanova K, Sanders HR, Gill SS. P-type Na⁺/K⁺-ATPase and V-type H⁺-ATPase expression patterns in the osmoregulatory organs of larval and adult mosquito *Aedes aegypti*. *J Exp Biol.* 2006; 209(Pt 23):4638–51. <https://doi.org/10.1242/jeb.02551> PMID: 17114398
23. Quijada-Rodriguez AR, Schultz AG, Wilson JM, He Y, Allen GJP, Goss GG, et al. Ammonia-independent sodium uptake mediated by Na⁺ channels and NHEs in the freshwater ribbon leech *Nephelopsis obscura*. *J Exp Biol.* 2017; 220(Pt 18):3270–9. <https://doi.org/10.1242/jeb.159459> PMID: 28684464
24. Quijada-Rodriguez AR, Treberg JR, Weihrauch D. Mechanism of ammonia excretion in the freshwater leech *Nephelopsis obscura*: characterization of a primitive Rh protein and effects of high environmental ammonia. *Am J Physiol Regul Integr Comp Physiol.* 2015; 309(6):R692–705. <https://doi.org/10.1152/ajpregu.00482.2014> PMID: 26180186
25. Shih TH, Horng JL, Hwang PP, Lin LY. Ammonia excretion by the skin of zebrafish (*Danio rerio*) larvae. *Am J Physiol Cell Physiol.* 2008; 295(6):C1625–32. <https://doi.org/10.1152/ajpcell.00255.2008> PMID: 18815227
26. Weihrauch D. Active ammonia absorption in the midgut of the tobacco hornworm *Manduca sexta* L.: Transport studies and mRNA expression analysis of a Rhesus-like ammonia transporter. *Insect Biochem Mol Biol.* 2006; 36(10):808–21. <https://doi.org/10.1016/j.ibmb.2006.08.002> PMID: 17027847
27. Weihrauch D, Ziegler A, Siebers D, Towle DW. Active ammonia excretion across the gills of the green shore crab *Carcinus maenas*: participation of Na⁺/K⁺-ATPase, V-type H⁺-ATPase and functional microtubules. *J Exp Biol.* 2002; 205(Pt 18):2765–75. PMID: 12177142
28. Weiner ID, Verlander JW. Role of NH₃ and NH₄⁺ transporters in renal acid-base transport. *Am J Physiol Renal Physiol.* 2011; 300(1):F11–23. <https://doi.org/10.1152/ajprenal.00554.2010> PMID: 21048022
29. Weiner ID, Verlander JW. Ammonia transport in the kidney by Rhesus glycoproteins. *Am J Physiol Renal Physiol.* 2014; 306(10):F1107–20. <https://doi.org/10.1152/ajprenal.00013.2014> PMID: 24647713
30. Wood CM, Nawata CM, Wilson JM, Laurent P, Chevalier C, Bergman HL, et al. Rh proteins and NH₄⁺-activated Na⁺-ATPase in the *Magadi tilapia* (*Alcolapia grahami*), a 100% ureotelic teleost fish. *J Exp Biol.* 2013; 216(Pt 16):2998–3007. <https://doi.org/10.1242/jeb.078634> PMID: 23885087
31. Worrell RT, Merk L, Matthews JB. Ammonium transport in the colonic crypt cell line, T84: role for Rhesus glycoproteins and NKCC1. *Am J Physiol Gastrointest Liver Physiol.* 2008; 294(2):G429–40. <https://doi.org/10.1152/ajpgi.00251.2006> PMID: 18032481
32. Gomes D, Agasse A, Thiébaud P, Delrot S, Geros H, Chaumont F. Aquaporins are multifunctional water and solute transporters highly divergent in living organisms. *Biochim Biophys Acta.* 2009; 1788(6):1213–28. <https://doi.org/10.1016/j.bbame.2009.03.009> PMID: 19327343
33. Fukasawa H, Bornheimer S, Kudlicka K, Farquhar MG. Slit diaphragms contain tight junction proteins. *J Am Soc Nephrol.* 2009; 20(7):1491–503. <https://doi.org/10.1681/ASN.2008101117> PMID: 19478094
34. Patari-Sampo A, Ihalmo P, Holthofer H. Molecular basis of the glomerular filtration: nephrin and the emerging protein complex at the podocyte slit diaphragm. *Ann Med.* 2006; 38(7):483–92. <https://doi.org/10.1080/07853890600978149> PMID: 17101539
35. Weavers H, Prieto-Sanchez S, Grawe F, Garcia-Lopez A, Artero R, Wilsch-Brauninger M, et al. The insect nephrocyte is a podocyte-like cell with a filtration slit diaphragm. *Nature.* 2009; 457(7227):322–6. <https://doi.org/10.1038/nature07526> PMID: 18971929
36. Raciti D, Reggiani L, Geffers L, Jiang Q, Bacchion F, Subrizi AE, et al. Organization of the pronephric kidney revealed by large-scale gene expression mapping. *Genome Biol.* 2008; 9(5):R84. <https://doi.org/10.1186/gb-2008-9-5-r84> PMID: 18492243
37. Scimone ML, Srivastava M, Bell GW, Reddien PW. A regulatory program for excretory system regeneration in planarians. *Development.* 2011; 138(20):4387–98. <https://doi.org/10.1242/dev.068098> PMID: 21937596
38. Thi-Kim Vu H, Rink JC, McKinney SA, McClain M, Lakshmanaperumal N, Alexander R, et al. Stem cells and fluid flow drive cyst formation in an invertebrate excretory organ. *eLife.* 2015; 4:e07405.
39. Greenberg JM. *Ex Bouillabaisse Lux: The Charm of Comparative Physiology and Biochemistry.* Amer Zool. 1985;(25):737–49.
40. Ruppert EE, Fox SF, Barnes DR. *Invertebrate Zoology, a functional evolutionary approach.* 7th ed. Belmont, CA: Brooks/Cole—Thomson Learning; 2004.
41. Wilson RA, Webster LA. Protonephridia. *Biol Rev.* 1974; 49(2):127–60. PMID: 4604982

42. Willmer EN. Cytology and Evolution. 2nd ed. New York, London: Academic Press; 1970.
43. Bartolomaeus T, Ax P. Protonephridia and Metanephridia—Their relation within the Bilateria. *Z Zool Syst Evol.* 1992; 30(1):21–45.
44. Goodrich ES. The study of nephridia and genital ducts since 1895. *Q J Microsc Sci.* 1945; 86:113–301. PMID: [21009526](#)
45. Kümmel G. Zwei neue Formen von Cyrtocyten. Vergleich der bisher bekannten Cyrtocyten und Erörterung des Begriffes 'Zelltyp'. *Zeitschr f Zellforsch.* 1962; 57:172–201.
46. Ruppert EE. Evolutionary Origin of the Vertebrate Nephron. *Am Zool.* 1994; 34(4):542–53.
47. Rouse GW, Wilson NG, Carvajal JI, Vrijenhoek RC. New deep-sea species of *Xenoturbella* and the position of Xenacoelomorpha. *Nature.* 2016; 530(7588):94–7. <https://doi.org/10.1038/nature16545> PMID: [26842060](#)
48. Ehlers U. Dermonephridia—modified epidermal cells with a probable excretory function in *Paratomella rubra* (Acoela, Plathelminthes). *Microfauna Mar.* 1992; 7:253–64.
49. Smith J III, Tyler S. The acoel turbellarians: kingpins of metazoan evolution or a specialized offshoot? In: Conway Morris S, George JD, Gibson R, Platt HM, editors. *The origins and relationships of lower invertebrates.* Oxford: Calderon Press; 1985. p. 123–42.
50. Weihrauch D, Allen GJP. Ammonia excretion in aquatic invertebrates: new insights and questions. *J Exp Biol.* 2018; 221(Pt 3):jeb169219.
51. Wall SM, Koger LM. NH₄⁺ transport mediated by Na⁺-K⁺-ATPase in rat inner medullary collecting duct. *Am J Physiol.* 1994; 267(4 Pt 2):F660–70. <https://doi.org/10.1152/ajprenal.1994.267.4.F660> PMID: [7943362](#)
52. Weihrauch D, Becker W, Postel U, Riestenpatt S, Siebers D. Active excretion of ammonia across the gills of the shore crab *Carcinus maenas* and its relation to osmoregulatory ion uptake. *Journal of comparative physiology B, Biochemical, systemic, and environmental physiology.* 1998; 168(5):364–76.
53. Weihrauch D, O'Donnell MJ. Links between Osmoregulation and Nitrogen-Excretion in Insects and Crustaceans. *Integ Comp Biol.* 2015; 55(5):816–29.
54. Kim HY, Verlander JW, Bishop JM, Cain BD, Han KH, Igarashi P, et al. Basolateral expression of the ammonia transporter family member Rh C glycoprotein in the mouse kidney. *Am J Physiol Renal Physiol.* 2009; 296(3):F543–55. <https://doi.org/10.1152/ajprenal.90637.2008> PMID: [19129254](#)
55. Pütter A. *Vergleichende Physiologie.* Jena: G. Fischer; 1911.
56. Macklin M. Osmotic regulation in *Hydra*: sodium and calcium localization and source of electrical potential. *J Cell Physiol.* 1967; 70(2):191–6. <https://doi.org/10.1002/jcp.1040700209> PMID: [4384472](#)
57. Lehnert EM, Mouchka ME, Burriesci MS, Gallo ND, Schwarz JA, Pringle JR. Extensive differences in gene expression between symbiotic and aposymbiotic cnidarians. *G3.* 2014; 4(2):277–95. <https://doi.org/10.1534/g3.113.009084> PMID: [24368779](#)
58. Moran Y, Genikhovich G, Gordon D, Wienkoop S, Zenkert C, Ozbek S, et al. Neurotoxin localization to ectodermal gland cells uncovers an alternative mechanism of venom delivery in sea anemones. *Proceedings B.* 2012; 279(1732):1351–8.
59. Biggs DC. Respiration and ammonium excretion by open ocean gelatinous zooplankton. *Limn Oceanog.* 1977; 22(1):108–17.
60. Matsakis S. Ammonia excretion rate of *Clytia* spp. hydromedusae (Cnidaria, Thecata): effects of individual dry weight, temperature and food availability. *Mar Ecol Prog Ser.* 1992; 87:55–63.
61. Burighel P, Cloney RA. Urochordata: Ascidiacea. In: Harrison FW, Ruppert EE, editors. *Microscopic Anatomy of Invertebrates* 15. New York: Wiley-Liss; 1997. p. 221–347.
62. Butt AG, Taylor HH. Salt and Water-Balance in the Spider, *Porrhothele antipodiana* (Mygalomorpha, Dipluridae)—Effects of Feeding Upon Hydrated Animals. *J Exp Biol.* 1986; 125:85–106.
63. Harpur RP. The nematode intestine and organic acid excretion: volatile acids in *Ascaris lumbricoides* faeces. *Comp Biochem Physiol.* 1969; 28(2):865–75. PMID: [5778267](#)
64. Nijhout HF. Excretory Role of Midgut in Larvae of Tobacco Hornworm, *Manduca-Sexta* (L). *J Exp Biol.* 1975; 62(1):221–30. PMID: [1151277](#)
65. Parry D. A. Habits, structure and development of *Spadella cephaloptera* and *Sagitta setosa*. *J Mar Biol Assoc.* 1944;(UK 26):16–36.
66. Phillips JE, Hanrahan J, Chamberlin M, Thomson B. Mechanisms and Control of Reabsorption in Insect Hindgut. *Adv Insect Physiol.* 1986; 19:329–422.
67. Tillinghast EK. Excretory pathways of ammonia and urea in the earthworm *Lumbricus terrestris*. *J Exp Zool.* 1967; 166(2):295–300. <https://doi.org/10.1002/jez.1401660213> PMID: [6080557](#)

68. Smith J III, Tyler S. The acoel turbellarians: kingpins of metazoan evolution or a specialized offshoot? In: Conway-Morris S, George JD, Gibson R, Platt HM, editors. The origins and relationships of lower invertebrates. Oxford: Oxford University Press; 1985.
69. Philippe H, Poustka AJ, Chiodin M, Hoff KJ, Dessimoz C, Tomiczek B, et al. Mitigating anticipated effects of systematic errors supports sister-group relationship between Xenacoelomorpha and Ambulacraria. *Curr Biol*. 2019; 29(11):1818–26 e6. <https://doi.org/10.1016/j.cub.2019.04.009> PMID: 31104936
70. Hejnal A, Martindale MQ. Acoel development supports a simple planula-like urbilaterian. *Philosophical transactions of the Royal Society of London Series B, Biological sciences*. 2008; 363(1496):1493–501. <https://doi.org/10.1098/rstb.2007.2239> PMID: 18192185
71. Koch M, Quast B, Bartolomaeus T. Coeloms and nephridia in annelids and arthropods. In: Wägele W, Bartolomaeus T, editors. *Deep Metazoan Phylogeny: The Backbone of the Tree of Life*. Berlin: De Gruyter; 2014. p. 173–284.
72. Andrikou C, Thiel D, Ruiz-Santesteban JA, Hejnal A. Active mode of excretion across digestive tissues predates the origin of excretory organs. 2019. Dryad Digital Repository. <https://doi.org/10.5061/dryad.bq068jr>.
73. Edgar RC. MUSCLE: multiple sequence alignment with high accuracy and high throughput. *Nucleic Acids Res*. 2004; 32(5):1792–7. <https://doi.org/10.1093/nar/gkh340> PMID: 15034147
74. Stamatakis A. RAxML version 8: a tool for phylogenetic analysis and post-analysis of large phylogenies. *Bioinformatics*. 2014; 30(9):1312–3. <https://doi.org/10.1093/bioinformatics/btu033> PMID: 24451623
75. Børve A, Hejnal A. Development and juvenile anatomy of the nemertodermatid *Meara stichopi* (Bock) Westblad 1949 (Acoelomorpha). *Front Zool*. 2014; 11.
76. De Mulder K, Kualess G, Pfister D, Willems M, Egger B, Salvenmoser W, et al. Characterization of the stem cell system of the acoel *Isodiametra pulchra*. *BMC Dev Biol*. 2009; 9.
77. Fritzenwanker JH, Technau U. Induction of gametogenesis in the basal cnidarian *Nematostella vectensis* (Anthozoa). *Dev Genes Evol*. 2002; 212(2):99–103. <https://doi.org/10.1007/s00427-002-0214-7> PMID: 11914942
78. Stephenson TA. *The British Sea Anemones*. London: The Ray Society; 1935.
79. Hejnal A, Martindale MQ. Acoel development indicates the independent evolution of the bilaterian mouth and anus. *Nature*. 2008; 456(7220):382–6. <https://doi.org/10.1038/nature07309> PMID: 18806777
80. Martín-Durán JM, Pang K, Børve A, Semmler LÊ H, Furu A, Cannon JT, et al. Convergent evolution of bilaterian nerve cords. *Nature*. 2018; 553(7686):45–50. <https://doi.org/10.1038/nature25030> PMID: 29236686
81. Genikhovich G, Technau U. In situ hybridization of starlet sea anemone (*Nematostella vectensis*) embryos, larvae, and polyps. *Cold Spring Harbor protocols*. 2009; 2009(9):pdb prot5282.
82. Chiodin M, Børve A, Berezikov E, Ladurner P, Martinez P, Hejnal A. Mesodermal gene expression in the acoel *Isodiametra pulchra* indicates a low number of mesodermal cell types and the endomesodermal origin of the gonads. *PLoS ONE*. 2013; 8(2):e55499. <https://doi.org/10.1371/journal.pone.0055499> PMID: 23405161
83. Sinigaglia C, Busengdal H, Leclere L, Technau U, Rentzsch F. The bilaterian head patterning gene *six3/6* controls aboral domain development in a cnidarian. *PLoS Biol*. 2013; 11(2):e1001488. <https://doi.org/10.1371/journal.pbio.1001488> PMID: 23483856
84. Schindelin J, Arganda-Carreras I, Frise E, Kaynig V, Longair M, Pietzsch T, et al. Fiji: an open-source platform for biological-image analysis. *Nat Methods*. 2012; 9(7):676–82. <https://doi.org/10.1038/nmeth.2019> PMID: 22743772